The ring finger protein 213 gene (Rnf213) contributes to Rift Valley fever resistance in mice

Denis Houzelstein, Dominique Simon-Chazottes, Leandro Batista, Satoko Tokuda, Francina Langa, Marie Flamand, Xavier Montagutelli, Jean-Jacques Panthier

The ring finger protein 213 gene (*Rnf213*) contributes to Rift Valley fever resistance in mice

Denis Houzelstein[1,2,5*], Dominique Simon-Chazottes[1,2], Leandro Batista[1,2], Satoko Tokuda[1,2], Francina Langa Vives[3], Marie Flamand[4], Xavier Montagutelli[1,2,6,7] and Jean-Jacques Panthier[1,2,7]

[1] Mouse Functional Genetics, Department of Developmental & Stem Cell Biology, Institut Pasteur, Paris, 75015, France.

[2] Centre National de la Recherche Scientifique, CNRS UMR3738, Paris, 75015, France.

[3] Mouse Genetics Engineering, Department of Developmental & Stem Cell Biology, Institut Pasteur, Paris, 75015, France.

[4] Structural Virology, Department of Virology, Institut Pasteur, Paris, 75015, France.

[5] Present address: Human Developmental Genetics, Department of Developmental & Stem Cell Biology, Institut Pasteur, Paris, 75015, France.

[6] Mouse Genetics, Institut Pasteur, Paris, 75015, France.

[7] These authors contributed equally.

*Corresponding author: denis.houzelstein@pasteur.fr

ORCID number

Denis Houzelstein 0000-0002-8536-9039

Xavier Montagutelli 0000-0002-9372-5398

Francina Langa Vives 0000-0002-0801-5464

Short Title: *Rnf213* promotes resistance to Rift Valley fever

Abstract

Rift Valley fever (RVF) is an emerging viral zoonosis that primarily affects ruminants and humans. We have previously shown that wild-derived MBT/Pas mice are highly susceptible to RVF virus and that part of this phenotype is controlled by a locus located on distal Chromosome 11. Using congenic strains, we narrowed down the critical interval to a 530 kb region containing five protein-coding genes among which *Rnf213* emerged as a potential candidate. We generated *Rnf213*-deficient mice by CRISPR/CAS9 on the C57BL/6J background and showed that they were significantly more susceptible to RVF than control mice, with an average survival time post-infection reduced from 7 to 4 days. The human *RNF213* gene had been associated with the cerebrovascular Moyamoya disease (MMD or MYMY) but the inactivation of this gene in the mouse resulted only in mild anomalies of the neovascularization. This study provides the first evidence that the *Rnf213* gene may also impact the resistance to infectious diseases such as RVF.

Keywords: Rift Valley Fever virus, Rnf213, infectious disease

Introduction

Rift Valley fever (RVF) is an emerging viral zoonosis caused by the RVF virus (RVFV) that primarily affects ruminants. A wide variation of symptoms is observed in infected animals, ranging from unapparent or moderate febrile reactions to high fever, severe prostration, and death in the most susceptible individuals (Ikegami and Makino 2011).

In humans, most RVF patients have no symptoms or present a self-limiting, febrile illness after a short incubation period of two to six days. Severe RVF disease accounts for 1-3% of infected individuals. It manifests itself by acute-onset liver disease, neurological disorders, vision loss, or hemorrhagic fever with a fatality rate of 10-20% in hospitalized individuals (Ikegami and Makino 2011). Little is known, however, of the natural host factors that influence the progression and severity of RVF disease in animals and humans.

Evidence from experimental models has demonstrated the importance of genetic host factors in determining RVF disease severity in mice (do Valle et al. 2010; Smith et al. 2010). We have previously shown that individuals of the MBT/Pas (MBT) inbred strain, which derives from wild progenitors of the *Mus musculus* (*M.m.*) *musculus* subspecies, exhibit earlier lethality than mice of the BALB/cByJ (BALB/c) inbred strain due to defective activation of the innate immune response (Ayari-Fakhfakh et al. 2012; do Valle et al. 2010). Quantitative trait locus (QTL) mapping identified three QTLs that contribute to RVF susceptibility in MBT mice (Tokuda et al. 2015). They were designated Rift Valley fever susceptibility 1 (*Rvfs1)*, *Rvfs2*, and

Rvfs3, and mapped on chromosome (Chr) 2, 11 and 5 respectively (Tokuda et al. 2015).

Differences in susceptibility to an infection may concern the mortality rate and/or the time to death, defined as the interval between infection and death in the mice succumbing to the infection. In our model of RVFV, we have often observed fluctuations in the mortality rate between experiments while the time to death has proven much more consistent. The *Rvfs2* locus was identified as strongly influencing the time to death, which has become the focus of our studies. Moreover, we have reported that, in our model, males were significantly more susceptible than females (Tokuda et al. 2015), therefore our recent studies were done on male mice.

The characterization of the Rvfs2 locus was achieved using congenic mice. Indeed, while most BALB/c males die from 9 to 10 days after infection with signs of encephalitis (Batista et al. 2020), C.MBT-*Rvfs2* congenic males, that carry the *Rvfs2* locus from the MBT strain on a BALB/c genetic background, generally die within 5 days of infection with signs of acute hepatitis. We have shown that the prolonged time to death in BALB/c mice could be explained by their capacity to overcome this acute hepatitis, emphasizing the pathophysiological relevance of the time to death as a parameter for suceptibility (Batista et al. 2020).

In the present study, we have refined the genetic mapping of the *Rvsf2* locus using overlapping subcongenic strains down to a 535-kb interval. Out of the five protein-coding genes contained in this critical interval, we identified *Rnf213* as potentially interacting with several genes of the innate immune response. *Rnf213* gene inactivation by a CRISP-Cas9-induced deletion resulted in a shorter survival time in

Rnf213-deficient mice compared with wild-type or heterozygous mice demonstrating a role for *Rnf213* in the resistance of this animal model to RVFV infection.

Results

Generation, characterization and fine-mapping of subcongenic strains delimitate the susceptibility interval within 535 kb

The *Rvfs2* QTL, which controls the average time to death in RVFV-lethally infected mice, was previously isolated in the C.MBT-*Rvfs2* congenic strain which carries a segment of ~16.9 Mb on distal Chr 11 (Tokuda et al. 2015). This strain now renamed C.MBT-*Rvfs2-1* was crossed with BALB/c mice to produce a series of subcongenic strains numbered C.MBT-*Rvfs2-2 (Rvfs2-2)* to C.MBT-*Rvfs2-8 (Rvfs2-8*) and shown in Figure 1A (see Table S1 for the list of markers used to map the recombination sites in the sub-congenic strains). Groups of homozygous subcongenic males were tested for their susceptibility to RVFV infection (Figure 1B). As previously observed, the average time to death in lethally-infected C.MBT-*Rvfs2-1* and BALB/c mice was 4.13 days and 7.38 days, respectively (Table 1). It appeared that the subcongenic strains could be sorted into two groups according to the average time to death : *Rvfs2-3* and *Rvfs2-7* (average time to death 8.06 and 6.78 days, respectively, as long as BALB/c mice), and all the other strains, namely *Rvfs2-2, Rvfs2-4, Rvfs2-5, Rvfs2-6,* and *Rvfs2-8*, in which susceptible mice died in less than 4.8 days, close to the *Rvfs2-1* congenic strain. Time to death was significantly longer in strains of the first group compared with the second group (Table 1) This result allowed us to narrow down the genomic interval containing the BALB/c resistance allele(s) to the interval spanning 535 kb between positions 119.393 and 119.928 Mb according to GRCm38-mm10 (Table S1). Analysis of the 535 kb susceptibility interval identified five protein-coding genes of known function (*Rnf213*, *EndoV*, *Nptx1*, *Rptor* and *Chmp6*), four long non-coding RNAs (*A930037H05Rik*, *Gm39484*, *Gm11762* and Gm39485), one antisense

long non-coding RNA (*Rptoros*) and one predicted sno RNA gene (*Gm23663*). To prioritize the genes most likely to be responsible for the phenotype of *Rvfs2-1* mice, we focused on protein-coding genes and used the STRING *Mus musculus* database to identify their interaction networks (Snel et al. 2000; Szklarczyk et al. 2015). This analysis, performed in April 2017, revealed that mouse RNF213 formed a highly interconnected network with UBA7, USP18, PARP14, IFIT3, IRF7, RSAD2, STAT1, IGTP, MX2, RTP4, OASL2, IRGM2, LGALS3BP, and OAS2 proteins (Figure S1). Seven of these 14 proteins were associated with the Gene Ontology (GO) categories 'innate immune response' (GO:0045087), 6 with 'immune effector process' (GO:0002252) and/or 'response to other organism' (GO:0051707), 5 with 'defense response to virus' (GO:0051607), 3 with 'negative regulation of viral process' (GO:0048525), and 2 with 'response to type I interferon' (GO:0034340). Considering its numerous interactions with innate immunity genes, we prioritized *Rnf213* for candidate gene studies.

Rnf213-deficient mice are more susceptible to RVFV infection

The mouse *Rnf213* gene encodes a 591-kDa cytosolic protein that possesses two main functional domains that we located by homology with other mammalian sequences (Figure 2A). The first domain (amino acids 2330 to 2964 of the mouse protein) is formed by a pair of AAA+ (ATPases associated with diverse cellular activities). ATPase modules are defined by specific structures surrounding Walker A and B motifs (Morito et al. 2014). It is encoded by exon 29 (Figures 2B and C). The second domain (amino acids 3877 to 3984) is a RING-finger-containing E3 ubiquitin ligase, PEX10 (COG5574) domain. It is encoded by exons 41 to 46 (Figure 2B).

Since the genome of the *Mus musculus musculus*-derived MBT/Pas strain has not been sequenced, we considered the PWK/PhJ strain, which belongs to the same subspecies, as a proxy for MBT/Pas. The sequence comparison between PWK/Pas and BALB/c strains (using the Sanger Institute's Mouse Genomes Project) identified 51 non-synonymous SNPs and 4 indels dispersed over most domains of the protein (Table S2). Eleven of these SNPs are located in splicing regions. Although variants between MBT/Pas and BALB/c may only partially overlap this set, these variants are too many to predict their cumulative functional impact (expression level, protein structure, stability or function).To assess the role of the *Rnf213* gene in RVFV infection, we produced *Rnf213*-deficient mice (referred to as $Rnf213^{tm3/tm3}$) by deleting the AAA+ domain encoding sequence (Figure 2C) and generating a frameshift by subsequent repair using non-homologous end joining (NHEJ, Figure 2C). The resulting truncated protein is predicted to contain neither of the two RNF213 characteristic conserved domains (Figure 2D).

Out of the founders obtained, two (#4 and 17) presented the expected truncation as revealed by sequencing and were used for strain establishment. Homozygous mutants did not show any visible phenotype under conventional environment as reported on previous $Rnf213^{tm/tm}$ mouse strains (Kobayashi et al. 2015; Sonobe et al. 2014).

After intra-peritoneal injection of 10^2 plaque-forming units (PFU) of the RVFV strain ZH548, about 13% of the C57BL/6J mice infected with RVFV survived the infection (2/15, Figure 3), not significantly different from that of $Rnf213^{tm3/tm3}$ (1/28 = 3.6%) and $Rnf213^{tm3/+}$ (0/10) mice (p=0.27 and p=0.5, respectively, Fisher's exact test).

However, the survival time in lethally infected mice was significantly shorter in *Rnf213*$^{tm3/tm3}$ (4.93 ± 0.28 days, mean ± s.e.m.) than in *Rnf213*$^{+/+}$ (7.15 ± 0.45 days, p=8.5 10^{-5}, Student's t-test) and *Rnf213*$^{tm3/+}$ (6.90 ± 0.28 days, p=2.7 10^{-4}) mice, resulting in highly significant differences in survival curves (Figure). Similar data were obtained with mutant mice of both #4 and 17 strains. These results indicate that the *Rnf213* gene delays the fatal outcome of RVFV infection in the C57BL/6J genetic background and that one functional allele is sufficient to confer this phenotype.

Discussion

Several studies by us and others have demonstrated that the outcome of RVFV infection is strongly influenced by multiple host genes. In particular, we have reported three RVF susceptibility loci affecting the time to death in susceptible mice (Tokuda et al. 2015). The *Rvfs2* locus was previously isolated in a congenic strain carrying a ~16.9 Mb segment of distal Chr 11 of the highy susceptible MBT strain in a BALB/c inbred background. We have previously shown that these congenic mice die earlier than BALB/c mice due to a higher susceptibility to the acute RVFV-induced hepatitis correlated with increased replication rate in hepatocytes (Batista et al. 2020). This result provided some functional evidence for the specific effect of the *Rvfs2* locus on the time to death in mice which develop a fatal infection.

In the present study, we aimed at identifying the genetic determinants responsible for the effect of *Rvfs2*. Genetic dissection of a large locus using subcongenic strains is a tedious process but also a rigourous approach for narrowing the position of causal variants. In our case, it allowed us to reduce the genomic interval down to

535 kb containing only 5 protein-coding genes, none of which had been so far involved in host genetic control of susceptibility to infections. We selected *Rnf213* as a candidate based on its interaction with several genes involved in the innate immune response. The production of a loss of function variant allowed us to assess the importance of *Rnf213* in the susceptibility to RVFV in mice.

Since the genome of the MBT strain has not been sequenced, we lack a comprehensive inventory of the variants between the MBT and BALB/c alleles of the *Rnf213* gene. However, the comparison between PWK/PhJ, a related inbred strain of the same mouse subspecies as MBT, and BALB/c revealed a large number of variants which could possibly alter the expression, protein structure or functional activity. Whether one or several of these genetic variants is responsible for the susceptibility to RVFV-induced acute hepatitis conferred by the *Rvfs2* locus remains to be determined. However, this hypothesis is reasonable since *Rnf213*-deficient mice show similar decrease of their survival time as C.MBT-*Rvfs2* mice.

Researchers have shown little interest in the human *RNF213* gene until 2011 when two groups independently demonstrated that SNPs in the gene were strongly associated with the onset of the cerebrovascular Moyamoya disease (MMD or MYMY) in both familial and sporadic cases ((Kamada et al. 2011; Liu et al. 2011), see (Koizumi et al. 2016; Lin and Sheng 2018) for reviews). Several variants of *RNF213* induce MYMY (MYMY2, OMIM #607151) with no other recognizable phenotypes. The disease was first described in Japan in 1957. It is a steno-occlusive disease of the cerebral arteries, involving smooth muscle cell proliferation with intima hyperplasia causing arterial stenosis and occlusion around the circle of Willis. This,

in turn, stimulates the compensatory development of collateral vessels, which have a ‘‘puff of smoke’’ (Moyamoya in Japanese) appearance in cerebral angiography (Koizumi et al. 2016; Lin and Sheng 2018). The mechanism by which *RNF213* variants relate to MYMY remains unknown. Knockdown of *RNF213* in cultured endothelial cells results in less angiogenic profiles suggesting that *RNF213* and its upstream pathways contribute to the process of angiogenesis (Ohkubo et al. 2015). Its expression is activated by inflammatory signals from the environment both *in vivo* and *in vitro*. Okhubo and colleagues therefore proposed that *RNF213* links inflammatory and angiogenic signals in endothelial cells (Ohkubo et al. 2015). The most frequent MYMY causing variant, R4810K, frequent in East Asian populations, has also been strongly associated with hypertension (Koizumi et al. 2013). At this stage, it is still difficult to link a role for *Rnf213* in the response to RVFV infection in mice and the documented role for *RNF213* in hypertension and angiopathies in humans.

RNF213 is an intracellular protein that forms large oligomers (Morito et al. 2014). It exerts ubiquitylation activity toward a variety of substrate proteins including itself (Kotani et al. 2017; Liu et al. 2011). RNF213 is targeted to lipid droplets, ubiquitous organelles specialized for neutral lipid storage, and markedly increases their abundance in cells (Sugihara et al. 2019). Depletion of RNF213 actually protects cells from palmitate-mediated cellular toxicity and normalizes the palmitate-induced changes in gene expression (Piccolis et al. 2019).

There are several stages during the course of RVFV infection where cellular lipids derived from *de novo* palmitate production are utilized. Reducing levels of fatty acid synthesis restricts RVFV infection in cell cultures. In contrast, restoring the level of

fatty acids by exogenous addition of palmitate, the first product of fatty acid biosynthesis, restores infection (Moser et al. 2012). Dependence on lipid biosynthesis and virally induced membrane modifications is not unique to RVFV; many RNA viruses require extensive membrane modifications and proliferations to support their replication complex (Filipe and McLauchlan 2015; Moser et al. 2012; Ogawa et al. 2009).

In human RVFV patients, the liver is the primary site of RVFV replication and lipid droplet accumulation was reported in the liver of a man who died from RVFV (Shraim et al. 2016). In the mouse model, a major consequence of RVFV infection is also the overwhelming infection of hepatocytes that subsequently undergo apoptosis resulting in early-onset death primarily attributed to severe hepatitis (Batista et al. 2020; Smith et al. 2010). The hepatocytes that maintain their viability amass cytoplasmic lipid droplets that persist during liver regeneration in the surviving mice (Reed et al. 2012). It is therefore possible that *Rnf213* influences resistance to RVFV infection through a role in lipid metabolism**.**

In conclusion, we have identified a new function for the *Rnf213* gene as a host factor controlling resistance to RVFV infections in mice. Review of the current literature suggests its effect may be mediated by a role in the lipid metabolism. It will therefore be of interest to determine whether *Rnf213* affects the infection outcome of other viruses in mouse models and whether *Rnf213* and its variants have an impact on susceptibility to viral infections in human as well.

Materials and Methods

Ethics statement

Experiments on mice were conducted according to the French and European regulations on care and protection of laboratory animals (EC Directive 2010/63/UE and French Law 2013-118 issued on February 1, 2013). The protocols were approved by the Animal Ethics Committees of Paris Center and South (N° 59) and of the Institut Pasteur (N° 89) and authorized by the French Ministry of Research (under references #06463 and 14646).

Mice

C57BL/6J mice were purchased from Janvier Labs (Le Genest-Saint-Isle, France). BALB/cByJ mice were purchased from Charles River Laboratories France (L'Arbresle, France). Subcongenic mice were obtained by backcrossing C.MBT-*Rvfs2-1* mice (similar to C.MBT-*Rvfs2* described by Tokuda *et al.* (Tokuda et al. 2015)) with BALB/cByJ mice and by genotyping progeny using polymorphic microsatellite or SNP markers. Several generations of backcrosses were necessary to obtain the recombination breakpoints present in C.MBT-*Rvfs2-2* to C.MBT-*Rvfs2-8* congenic strains.

Virus production and mouse infection

The RVFV strain ZH548, isolated from a male patient with the acute febrile illness at Zagazig fever hospital, Egypt (El-Akkad 1978; Meegan 1979), obtained from *Centre National de Référence des Fièvres Hémorragiques Virales, Institut Pasteur, Lyon, France*, was used for all infection studies. All experiments that involved virulent RVFV were performed in the biosafety level 3 (BSL3) facilities of the Institut Pasteur, and carried out in compliance with the recommendations of the Institut Pasteur

Biosafety Committee (N° 14.320). Stocks of RVFV ZH548 were titrated by plaque assay on monolayers of Vero E6 cells (Billecocq et al. 2008). Nine to thirteen weeks old male mice were infected by intraperitoneal (i.p.) injection of 10^2 PFU RVFV. Morbidity and mortality were monitored daily for 11 to 14 days following infection.

Generation of CRISPR/Cas9 mutants

Single guide RNAs (sgRNAs) were prepared according to (Cong et al. 2013), as described by Raveux *et al.* (Raveux et al. 2017). For each guide sequence, an oligonucleotide pair was annealed and cloned into a *Bbs*I-digested pX458 expression vector. After sequencing, PCR products were used as templates with MEGAshortscript T7 and mMESSAGE mMACHINE T7 transcription kits (Life Technologies, Carlsbad, CA, USA) for the guides and Cas9, respectively. sgRNAs and Cas9 mRNA were then precipitated with LiCl/ethanol and resuspended in Brinster's buffer (10 mM Tris-HCl pH 7.5, 0.25 mM EDTA).

To increase the probability of obtaining non-homologous end joining events, we designed 4 guides in the exon 29 of *Rnf213* which encodes the tandem AAA+ ATPase domains. Two guides target sequences 5' to the AAA+ ATPase domains (5'-1: TTAAATACTGGTAAGGTCGT**TGG** and 5'-2: CACTTCCTTGGGAGGACGGC**AGG**), whereas the remaining two guides target sequences 3' to the AAA+ ATPase domains (3'-1: TGTGCCCCTCATCAACCGTC**TGG** and 3'-2: CTCGATGACGATGAGGCGGA**AGG**). The guides (50ng/µl each) and Cas9 mRNA (100ng/µl) were microinjected into C57BL/6J one-cell-stage embryos. The resulting pups were screened by PCR with three primers (rnf213-diag5L-1f: TGTGTTAGAAAATGCATCTTTGTTAGGG, rnf213-diag3C-1f: TGCTCTCAACCAGTACTATGTCTACCTTGG, and rnf213-diag3C-1r: CAATGAACTGGTCTGCTTTTACATCTGCG). The predicted PCR products of the wild-

type and mutant alleles were 281 bp (rnf213-diag5L-1f_ rnf213-diag3C-1r) and 450bp (rnf213-diag3C-1f_ rnf213-diag3C-1r) in length, respectively (Figure 2C). Exon 29 was sequenced in several mutants to confirm the predicted deletion (Figure 2D). The sequence of the RNF213^{tm3} proteins is shown in Figure 2E.

Statistical analysis

Gehan-Breslow-Wilcoxon test for survival analysis and Fisher's exact test were performed using GraphPad Prism version 8.4.1 for MacOS (GraphPad Software, La Jolla California USA).

DATA AVAILABILITY STATEMENT

All relevant data are within the article

CONFLICT OF INTEREST

The authors declare no conflict of interest.

ACKNOWLEDGMENTS

We are grateful to all members of the laboratory for technical advice and helpful discussion. We are grateful to Lauranne Machou and María Bernad Roche for their precious help during their short stay in the laboratory. . We would like to thank the members of the Mouse Genetics Engineering Center, Sébastien Chardenoux, Ilta Lafosse, and Gaëlle Chauveau Le Friec for technical support with transgenic mice. This work was supported by the *Agence Nationale de la Recherche* (grant n° 11-BSV3-007 01, 'GenRift') and the French Government's Investissement d'Avenir program, Laboratoire d'Excellence Integrative Biology of Emerging Infectious Diseases (grant n°ANR-10-LABX-62-IBEID).

AUTHOR CONTRIBUTION

Denis Houzelstein conceived the study, performed the experiments, analysed the data, and wrote the manuscript.
Dominique Simon-Chazottes performed *in vivo* experiments.
Leandro Batista and Satoko Tokuda produced congenic strains.
Francina Langa Vives and her team produced the *Rnf213*^{tm3} founder individuals.
Marie Flamand and her team assisted with RVFV production and titration.
Xavier Montagutelli assisted with data analysis, performed *in vivo* experiments, and wrote the manuscript.
Jean-Jacques Panthier provided funding, conceived the study, and wrote the manuscript.

FIGURE LEGENDS

Figure 1.

A. Schematic representation of the genomic intervals harbored by the congenic *Rvfs2-1* and the subcongenic *Rvfs2-2* to *Rvfs2-8* strains produced to fine map the *Rvfs2* QTL. The black bars represent the regions homozygous for the BALB/c genome (the background strain) and the grey bars represent the regions homozygous for the donor MBT genome. E: eary lethality (similar to *Rvfs2.1*); L: late lethality (similar to BALB/c). On the right are shown the approximate positions of the boundaries of the minimal interval and the genes it contains.

B. Survival curves of C.MBT-*Rvfs2* congenic and subcongenic (*Rvfs2-1* to *Rvfs2-8*) and BALB/c mice after infection with 100 PFU of RVFV ZH548 strain. Numbers of mice are given in brackets.

Figure 2.

Structure of the *Rnf213* gene and the CRISP-Cas9-induced mutation. **A:** Organization of the RNF213 protein. The position of the RNF213 conserved domains is indicated. **B:** Structure of the endogenous mouse *Rnf213* gene highlighting the position of exon 29 which encodes the AAA+ domains. **C:** The guides used to generate the deleted allele are shown as black arrows relative to the AAA+ domains. The primers used for genotyping transgenic mice are shown in red with the expected amplicon size. The expected deletion is shown as a triangle. PCR genotyping of $Rnf213^{+/+}$, $Rnf213^{tm3/tm3}$ (Δ/Δ) and $Rnf213^{+/tm3}$ mice using primers: diag5L-1f, diag3C-1F and diag3C-1r . **D:** Genomic deletion in the two $Rnf213^{tm3}$ alleles analyzed. $Rnf213^{tm3}$-17

carries a 6 base pair insertion within the deletion. **E:** Amino acid sequence of the C57BL/6J Rnf213 protein and of the truncated protein predicted from the deleted nucleotide sequence of the *Rnf213*$^{tm3/tm3}$-4 and *Rnf213*$^{tm3/tm3}$-17 mutants.

Figure 3.

Survival curves of *Rnf213*$^{tm3/tm3}$, *Rnf213*$^{tm3/+}$, and C57BL/6J (*Rnf213*$^{+/+}$) male mice after infection with 100 PFU of RVFV ZH548 strain. Numbers of mice are given in brackets. Statistical test: Gehan-Breslow-Wilcoxon test, ***(1) p=0.0002, ***(2) p=0,0010.

Table 1.

§ comparison of the survival time between the first group of strains (BALB/cByJ, C.MBT-*Rvfs2-3* and C.MBT-*Rvfs2-7*) and all the others; strains of the second group did not statistically differ between them; numbers refer to C.MBT-*Rvfs2* substrains; **: p<0.01; ***: p<0.001; ****: p<0.0001.

References

Ayari-Fakhfakh E, do Valle TZ, Guillemot L, Panthier JJ, Bouloy M, Ghram A, Albina E, Cetre-Sossah C (2012) MBT/Pas mouse: a relevant model for the evaluation of Rift Valley fever vaccines. The Journal of general virology 93, 1456-1464

Batista L, Jouvion G, Simon-Chazottes D, Houzelstein D, Burlen-Defranoux O, Boissière M, Tokuda S, do Valle TZ, Cumano A, Flamand M, Montagutelli X, Panthier J-J (2020) Genetic dissection of Rift Valley fever pathogenesis: Rvfs2 locus on mouse chromosome 11 enables survival to early-onset hepatitis. Scientific Reports 10

Billecocq A, Gauliard N, Le May N, Elliott RM, Flick R, Bouloy M (2008) RNA polymerase I-mediated expression of viral RNA for the rescue of infectious virulent and avirulent Rift Valley fever viruses. Virology 378, 377-384

Cong L, Ran FA, Cox D, Lin SL, Barretto R, Habib N, Hsu PD, Wu XB, Jiang WY, Marraffini LA, Zhang F (2013) Multiplex Genome Engineering Using CRISPR/Cas Systems. Science 339, 819-823

do Valle TZ, Billecocq A, Guillemot L, Alberts R, Gommet C, Geffers R, Calabrese K, Schughart K, Bouloy M, Montagutelli X, Panthier JJ (2010) A New Mouse Model Reveals a Critical Role for Host Innate Immunity in Resistance to Rift Valley Fever. The Journal of Immunology 185, 6146-6156

El-Akkad AM (1978) Rift Valley fever outbreak in Egypt. October--December 1977. The Journal of the Egyptian Public Health Association 53, 123-128

Filipe A, McLauchlan J (2015) Hepatitis C virus and lipid droplets: finding a niche. Trends Mol Med 21, 34-42

Ikegami T, Makino S (2011) The Pathogenesis of Rift Valley Fever. Viruses 3, 493-519

Kamada F, Aoki Y, Narisawa A, Abe Y, Komatsuzaki S, Kikuchi A, Kanno J, Niihori T, Ono M, Ishii N, others (2011) A genome-wide association study identifies RNF213 as the first Moyamoya disease gene. Journal of human genetics 56, 34-40

Kobayashi H, Matsuda Y, Hitomi T, Okuda H, Shioi H, Matsuda T, Imai H, Sone M, Taura D, Harada KH, Habu T, Takagi Y, Miyamoto S, Koizumi A (2015) Biochemical and Functional Characterization of RNF213 (Mysterin) R4810K, a Susceptibility Mutation of Moyamoya Disease, in Angiogenesis In Vitro and In Vivo. Journal of the American Heart Association: Cardiovascular and Cerebrovascular Disease 4, e002146

Koizumi A, Kobayashi H, Hitomi T, Harada KH, Habu T, Youssefian S (2016) A new horizon of moyamoya disease and associated health risks explored through RNF213. Environmental Health and Preventive Medicine 21, 55-70

Koizumi A, Kobayashi H, Liu W, Fujii Y, Senevirathna ST, Nanayakkara S, Okuda H, Hitomi T, Harada KH, Takenaka K, Watanabe T, Shimbo S (2013) P.R4810K, a polymorphism of RNF213, the susceptibility gene for moyamoya disease, is associated with blood pressure. Environ Health Prev Med 18, 121-129

Kotani Y, Morito D, Sakata K, Ainuki S, Sugihara M, Hatta T, Iemura S-i, Takashima S, Natsume T, Nagata K (2017) Alternative exon skipping biases substrate preference of the deubiquitylase USP15 for mysterin/RNF213, the moyamoya disease susceptibility factor. Scientific Reports 7, 44293

Lin J, Sheng W (2018) RNF213 Variant Diversity Predisposes Distinct Populations to Dissimilar Cerebrovascular Diseases. Biomed Res Int 2018, 6359174

Liu W, Morito D, Takashima S, Mineharu Y, Kobayashi H, Hitomi T, Hashikata H, Matsuura N, Yamazaki S, Toyoda A, Kikuta K-i, Takagi Y, Harada KH, Fujiyama A, Herzig R, Krischek B, Zou L, Kim JE, Kitakaze M, Miyamoto S, Nagata K, Hashimoto N, Koizumi A (2011)

Identification of RNF213 as a Susceptibility Gene for Moyamoya Disease and Its Possible Role in Vascular Development. PLoS ONE 6, e22542
Meegan JM (1979) The Rift Valley fever epizootic in Egypt 1977-78. 1. Description of the epizzotic and virological studies. Transactions of the Royal Society of Tropical Medicine and Hygiene 73, 618-623
Morito D, Nishikawa K, Hoseki J, Kitamura A, Kotani Y, Kiso K, Kinjo M, Fujiyoshi Y, Nagata K (2014) Moyamoya disease-associated protein mysterin/RNF213 is a novel AAA+ ATPase, which dynamically changes its oligomeric state. Scientific Reports 4
Moser TS, Schieffer D, Cherry S (2012) AMP-Activated Kinase Restricts Rift Valley Fever Virus Infection by Inhibiting Fatty Acid Synthesis. PLoS Pathogens 8, e1002661
Ogawa K, Hishiki T, Shimizu Y, Funami K, Sugiyama K, Miyanari Y, Shimotohno K (2009) Hepatitis C virus utilizes lipid droplet for production of infectious virus. Proc Jpn Acad Ser B Phys Biol Sci 85, 217-228
Ohkubo K, Sakai Y, Inoue H, Akamine S, Ishizaki Y, Matsushita Y, Sanefuji M, Torisu H, Ihara K, Sardiello M, Hara T (2015) Moyamoya disease susceptibility gene RNF213 links inflammatory and angiogenic signals in endothelial cells. Scientific Reports 5, 13191
Piccolis M, Bond LM, Kampmann M, Pulimeno P, Chitraju C, Jayson CBK, Vaites LP, Boland S, Lai ZW, Gabriel KR, Elliott SD, Paulo JA, Harper JW, Weissman JS, Walther TC, Farese RV, Jr. (2019) Probing the Global Cellular Responses to Lipotoxicity Caused by Saturated Fatty Acids. Mol Cell
Raveux A, Vandormael-Pournin S, Cohen-Tannoudji M (2017) Optimization of the production of knock-in alleles by CRISPR/Cas9 microinjection into the mouse zygote. Sci Rep 7, 42661
Reed C, Steele KE, Honko A, Shamblin J, Hensley LE, Smith DR (2012) Ultrastructural study of Rift Valley fever virus in the mouse model. Virology 431, 58-70
Shraim MA, Eid R, Radad K, Saeed N (2016) Ultrastructural pathology of human liver in Rift Valley fever. BMJ Case Rep 2016
Smith DR, Steele KE, Shamblin J, Honko A, Johnson J, Reed C, Kennedy M, Chapman JL, Hensley LE (2010) The pathogenesis of Rift Valley fever virus in the mouse model. Virology 407, 256-267
Snel B, Lehmann G, Bork P, Huynen MA (2000) STRING: a web-server to retrieve and display the repeatedly occurring neighbourhood of a gene. Nucleic acids research 28, 3442-3444
Sonobe S, Fujimura M, Niizuma K, Nishijima Y, Ito A, Shimizu H, Kikuchi A, Arai-Ichinoi N, Kure S, Tominaga T (2014) Temporal profile of the vascular anatomy evaluated by 9.4-T magnetic resonance angiography and histopathological analysis in mice lacking RNF213: A susceptibility gene for moyamoya disease. Brain Research 1552, 64-71
Sugihara M, Morito D, Ainuki S, Hirano Y, Ogino K, Kitamura A, Hirata H, Nagata K (2019) The AAA+ ATPase/ubiquitin ligase mysterin stabilizes cytoplasmic lipid droplets. J Cell Biol 218, 949-960
Szklarczyk D, Franceschini A, Wyder S, Forslund K, Heller D, Huerta-Cepas J, Simonovic M, Roth A, Santos A, Tsafou KP, Kuhn M, Bork P, Jensen LJ, von Mering C (2015) STRING v10: protein-protein interaction networks, integrated over the tree of life. Nucleic acids research 43, D447-452
Tokuda S, Do Valle TZ, Batista L, Simon-Chazottes D, Guillemot L, Bouloy M, Flamand M, Montagutelli X, Panthier JJ (2015) The genetic basis for susceptibility to Rift Valley fever disease in MBT/Pas mice. Genes and Immunity 16, 206-212

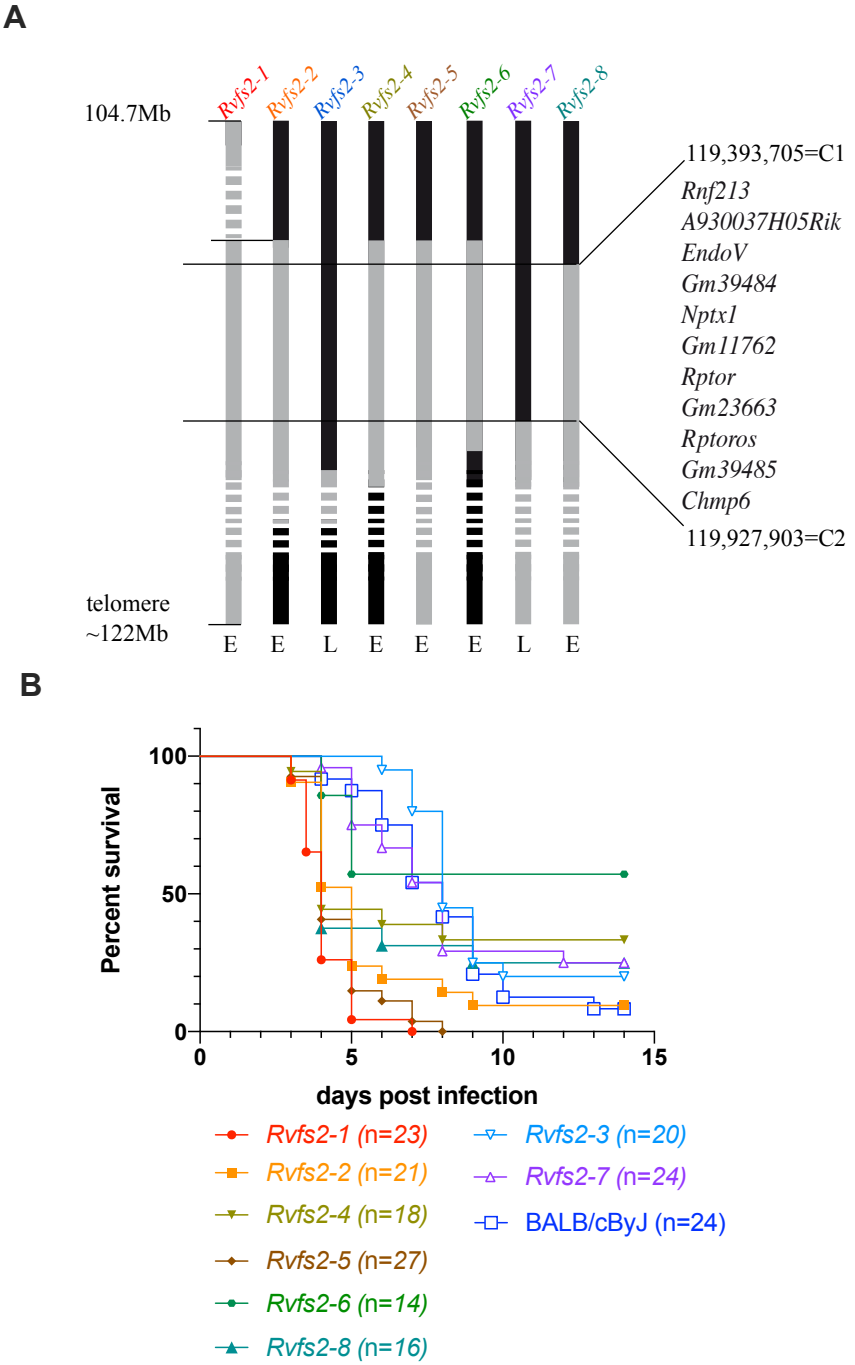

Figure 1.

A. Schematic representation of the genomic intervals harbored by the congenic *Rvfs2-1* and the subcongenic *Rvfs2-2* to *Rvfs2-8* strains produced to fine map the *Rvfs2* QTL. The black bars represent the regions homozygous for the BALB/c genome (the background strain) and the grey bars represent the regions homozygous for the donor MBT genome. E: eary lethality (similar to *Rvfs2.1*); L: late lethality (similar to BALB/c). On the right are shown the approximate positions of the boundaries of the minimal interval and the genes it contains.

B. Survival curves of C.MBT-*Rvfs2* congenic and subcongenic (*Rvfs2-1* to *Rvfs2-8*) and BALB/c mice after infection with 100 PFU of RVFV ZH548 strain. Numbers of mice are given in brackets.

Table 1 : Survival time in lethally-infected mice

Mouse strain	Survival time in days mean ± s.e.m.	Comparisons[§] (Mann-Whitney)
BALB/cByJ	7.38 ± 0.39	1, 2, 4, 5, 8: **** 6: **
C.MBT-*Rvfs2-3*	8.06 ± 0.25	1, 2, 4, 5, 6, 8: **** 7: **
C.MBT-*Rvfs2-7*	6.78 ± 0.45	1, 5: **** 2, 4, 8: *** 3, 6: **
C.MBT-*Rvfs2-1*	4.13 ± 0.18	
C.MBT-*Rvfs2-2*	4.79 ± 0.35	
C.MBT-*Rvfs2-4*	4.33 ± 0.31	
C.MBT-*Rvfs2-5*	4.63 ± 0.23	
C.MBT-*Rvfs2-6*	4.67 ± 0.21	
C.MBT-*Rvfs2-8*	4.58 ± 0.43	

[§] comparison of the survival time between the first group of strains (BALB/cByJ, C.MBT-*Rvfs2-3* and C.MBT-*Rvfs2-7*) and all the others; strains of the second group did not statistically differ between them; numbers refer to C.MBT-*Rvfs2* substrains; **: p<0.01; ***: p<0.001; ****: p<0.0001.

Table 1.

[§] comparison of the survival time between the first group of strains (BALB/cByJ, C.MBT-*Rvfs2-3* and C.MBT-*Rvfs2-7*) and all the others; strains of the second group did not statistically differ between them; numbers refer to C.MBT-*Rvfs2* substrains; **: p<0.01; ***: p<0.001; ****: p<0.0001.

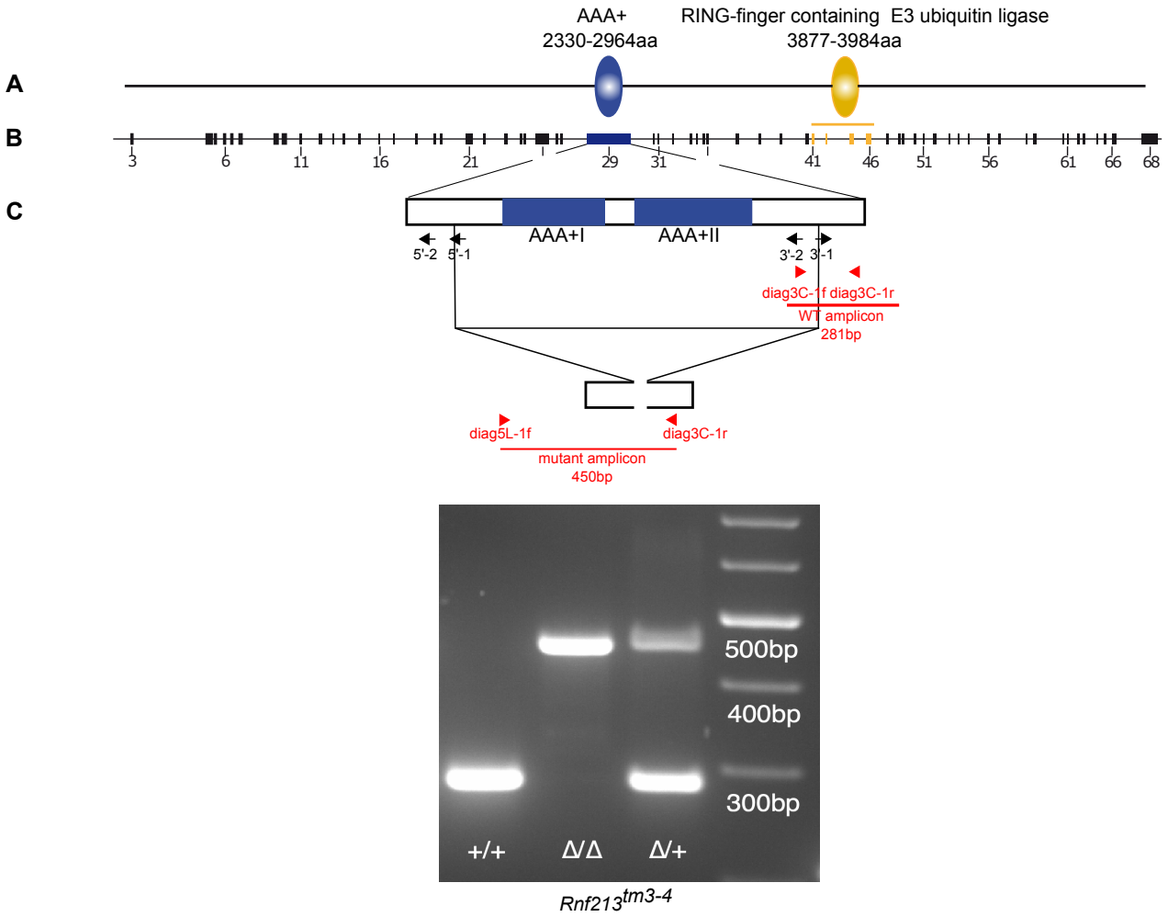

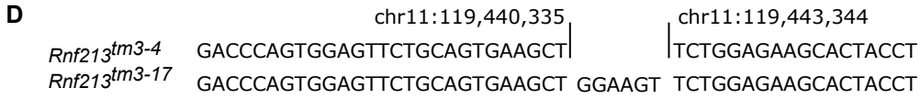

Figure 2.

Structure of the *Rnf213* gene and the CRISP-Cas9-induced mutation. **A:** Organization of the RNF213 protein. The position of the RNF213 conserved domains is indicated. **B:** Structure of the endogenous mouse *Rnf213* gene highlighting the position of exon 29 which encodes the AAA+ domains. **C:** The guides used to generate the deleted allele are shown as black arrows relative to the AAA+ domains. The primers used for genotyping transgenic mice are shown in red with the expected amplicon size. The expected deletion is shown as a triangle. PCR genotyping of *Rnf213*$^{+/+}$, *Rnf213*$^{tm3/tm3}$ (Δ/Δ) and *Rnf213*$^{+/tm3}$ mice using primers: diag5L-1f, diag3C-1F and diag3C-1r . **D:** Genomic deletion in the two *Rnf213*^{tm3} alleles analyzed. *Rnf213*^{tm3}-17 carries a 6 base pair insertion within the deletion. **E:** Amino acid sequence of the C57BL/6J Rnf213 protein and of the truncated protein predicted from the deleted nucleotide sequence of the *Rnf213*$^{tm3/tm3}$-4 and *Rnf213*$^{tm3/tm3}$-17 mutants.

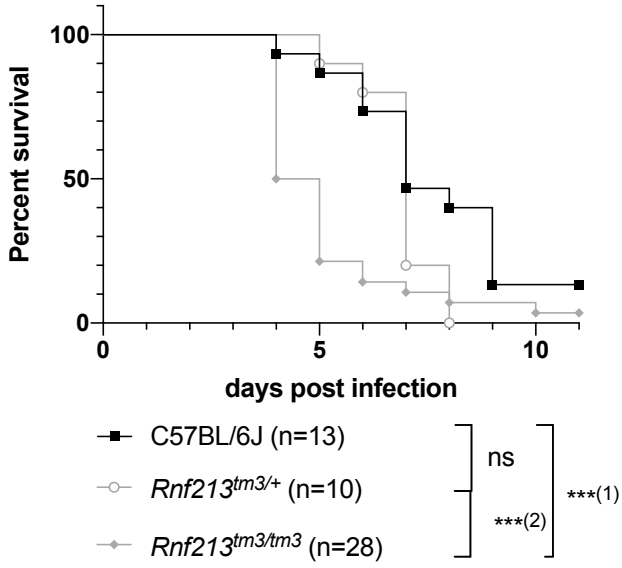

Figure 3.

Survival curves of *Rnf213*$^{tm3/tm3}$, *Rnf213*$^{tm3/+}$, and C57BL/6J (*Rnf213*$^{+/+}$) male mice after infection with 100 PFU of RVFV ZH548 strain. Numbers of mice are given in brackets. Statistical test: Gehan-Breslow-Wilcoxon test, ***$^{(1)}$ p=0.0002, ***$^{(2)}$ p=0,0010.

Table S1. Markers used to build the physical map of the C.MBT-*Rvfs2* subcongenic strains.

Name	Position*	rvfs2-2	rvfs2-3	rvfs2-4	rvfs2-5	rvfs2-6	rvfs2-7	rvfs2-8	Primer sequence	Amplicon	Band size
slc26a11-1f	119 357 215			M	c	M	c	c	GCGGTCCTAGATTTTCCAACTGGGG	amplicon: 416pb -followed by restriction with NlaIII	BALB: 32pb + 7pb +307pb + 76pb
slc26a11-1r	119 357 630								TCTGAGTGTCTGGAACTGAACCCCG		PWK: 32pb + 7pb +365pb
slc26a11-2f	119 380 672								TCTAATCTGAGCTGAAGAGGTGGCC	PWK: 832 pb BALB: 841	
slc26a11-2r	119 381 506								CGCCCATATACAGTGTTGGATGGGG		
Mir1932-2f	119 385 695	M	c	M	M	M	c	c	GGCTAGAATGTGTAAGTTTTGTAATTCTGG	BALB: 395, MBT: 210	
Mir1932-2r	119 386 089								CCTTGGGGCAAATTTGATCTCCACC		
mf213-2f	119 392 890		c			M		c	TTGGGGGAGTAGCTGGACTTGAGTTAGAGC	amplicon: 291pb -followed by restriction with NlaIII	BALB: 212pb+22pb+56pb
mf213-2r	119 393 180								AGAAGGCAATTTCTGTCCGCACTCG		PWK: 138pb+74pb+22pb+56pb
Rnf213-exon00-1f	119 392 806								CTTTTGAGCTTCCCTGGGCTTCG	amplicon: 900pb - sequenced	
Rnf213-exon00-1r	119 393 705							c	GTGCTCTTCACTGCATAGGCCATCC		C1
mf213-1f	119 400 214	M	c	M	M	M	c	M	GACAGTAGGAATGGTTTTGGGAAGG	PWK: 545pb BALB: 739pb	
mf213-1r	119 400 952								CCCACTGCTGTAACAAATCTTGTCC		
EndoV-1f	119 528 452						c	M	GCCAGTATTGAGTGTGGTTCCTCCC	PWK: 180 pb BALB: 159 pb	
EndoV-1r	119 528 631								GTCCACTCAGAACCTGTGAATGGGG		
Nptx1-1f	119 547 995						c	M	CCGAAGACTACCAGAATACAGGGCC	amplicon: 636pb -followed by restriction with NlaIII	BALB: 172pb + 102pb +361pb
Nptx1-1r	119 548 631								TTCAAGTGGACCGGTAAACCCAACG		PWK: 172pb + 463pb
Gm11762-1f	119 570 841						c	M	AGCAAGTGACCAGTTGACAGGAAGC	PWK: 419pb BALB: 297pb	
Gm11762-1r	119 571 260								CCTCACCATGGTCAGGGCTTTACC		
Rptor-1f	119 861 491	M	c	M	M	M	c	M	ATGGTCTCACTTCAAAGCCACTGGG	PWK: 248pb BALB: ~300pb	
Rptor-1r	119 861 882								GAACGAACACAGGATCAGGGCTCTG		
Rptor-2f	119 899 881						c	M	CTACCCACTGCGAATGTCTCCATCC	amplicon: 158pb -followed by restriction with NlaIII	BALB: 117pb + 16pb
Rptor-2r	119 900 038								ACCCTGACACCTGAGGTATCCTTCC		PWK: 85pb + 32pb +16pb
Chmp6-2f	119 911 581						c		TTCCCTCCTTTCAGGTGACTCTGGC	PWK: 339pb BALB: 395pb	
Chmp6-2r	119 911 975								CTTCCCTTTGCCTCCCTTTGCTGG		
Chmp6-3f	119 917 845						c		CAGGGCCAGTCATCTGAGCAGG	amplicon: 248pb -followed by restriction with NlaIII	BALB: 118+130
Chmp6-3r	119 918 092								GGGTATGTTCCTTAGACCAACACG		PWK: 248
Chmp6-1f	119 927 903		c	M		M	M		TGTGATTCCAAAGGAAAAGACAGTCC	PWK: 280 pb BALB 346 pb	C2
Chmp6-1r	119 928 248								TTTAAATTTGTAAACTGATGCCTTTCGC		
Baiap-1f	120 006 436					M		M	CTCTGCATCGACACTCTGTCCCC	amplicon: 149pb followed by restriction with NlaIII	BALB: 51pb + 97pb
Baiap-1r	120 006 584								CAGCCACCTCACCAGGAACACC		PWK:51pb + 25pb + 72pb
Aatk-1f	120 014 703	M	c	M	M	c	M	M	CTACCCCAGGAGGACTGTGTCAGG	PWK: 127pb BALB: 180pb	
Aatk-1r	120 014 743								GTCCTCCCCAACAATATCCTGGTGC		
Azi1-2f	120 064 310		c	M		c			AGTCGGAGCTAGTCCTGCAGTAAGG	amplicon: 820 pb - sequenced	
Azi1-2r	120 065 129								TAGCCACCCAGAGTCTCCTTAGTCC		
Azi1-3f	120 085 919		c			c		M	CTAGGACTCCCTTGAGAGGACAGGG	amplicon: 161 pb -followed by restriction with NlaIII	BALB: 92pb + 65pb
Azi1-3r	120 086 079								GACCATGGTGAGTGTATGCTCCTGG		PWK:157pb
11-rik120,1-1f	120 099 574		M			c		M	CATGACCCCTCCACTAGAGCTAGGG	amplicon :243pb -followed by restriction with NlaIII	BALB: 243pb
11-rik120,1-1r	120 099 816								TGGCCACCAACCACAAGAGTAAAGG		PWK: 140pb +102pb
slc38a10-1f	120 101 727	M	M	M	M	c	M	M	GGCTCTTACTATGACCCAGAGCAGC	PWK:198pb BALB: 379pb	
slc38a10-1r	120 102 105								CTTGAAGATGACACTGGCAGGTTGG		
Actg1-1f	120 341 838	M	M	c	M	c	M	M	CAGTGCTGGACTTGAAGGAGACTGG	PWK: 338pb, BALB: 725pb	
Actg-1r	120 342 562								TCTCTCCAGCCCTCTACCCCTTATT		
Nploc4-1f	120 424 100	M	M	c	M	c	M	M	CGCTTTGGTTAGGCCTAGTGGTTCA	PWK: 212pb, BALB: 409pb	
Nploc4-1r	120 424 508								ATGGACAGGGGACAAAACACGAGAC		
ccdc137-1f	120 460 307	M	M	c	M	c	M	M	TGGTGACTGTGTCCTCTGGTGATAG	PWK: 400 BALB: 586pb	
ccdc137-1r	120 460 892								TGTCCTGTTCTTAGACCCTCCAGTG		
P4hb-1f	120 568 970	M	M	c	M	c	M	M	ACAGCTCACTCAGAGAACCCAGAGC	PWK: 600 BALB: 400	
P4hb-1r	120 569 573								CGGCACCAGTCAAAAATTTAAAGG		
Cbr2-1f	120 735 744	M	M	c	M	c	M	M	GGCCTTACAGCTGGATCTCATGAAGG	PWK: 368pb BALB: 776pb	
Cbr2-1r	120 736 519								GAGTTGGAGAAGTCACCCAATCCCG		
cd7-1f	121 043 129	M	M	c	M	c	M	M	AATGAGTTCACCTGGACCCACTAGC	MBT:150pb BALB: 300pb	
cd7-1r	121 043 421								CTAGACGTGGACTAGGAAGCCCAAT		
Sectm1a-1f	121 095 593	M	M	c	M	c	M	M	TCAGGCAAGGGTTGTGAAAGTTGGG	MBT: <<300pb BALB: -	
Sectm1a-1r	121 096 410								ATGACTTTAGTCCCAGCCCTCCAGA		
Tex19.2-1f	121 126 146	M	M	c	M	c			TCAGGACTCTTCACAGGTTGCAGAC	MBT: 1.2kb PWK: 214 BALB: 1437bp	
Tex19.2-1r	121 127 582								GGGTTACCACTTTCTGCTCAGGGTT		
Tex19.1-1f	121 152 273	M	M	c	M	c			ACAAGCCAAGCTCTGTCTCCATCAC	MBT: ~550pb PWK: 441pb BALB: 585pb	
Tex19.1-1r	121 152 857								CCCAACCGTTGTGTTAGAACCTGGT		
Hexdc -1f	121 217 621	c	c	c	M	c	M	M	CCCAAAACACAGAAACACAGCTGCA	PWK: 367pb BALB: 549pb	
Hexdc -1r	121 218 169								CCGTACTGACCTTTGCCATGGACAT		
Narf-1f	121 247 120	c	c	c	M	c	M	M	TCAGTGGCCTAAAGTGAAGAAGAAGG	PWK: 230 BALB: 486	
Narf-1r	121 247 605								ACATATGGCTTCCTCCCTAAGATGG		
Foxk2-1f	121 323 858	c	c	c	M	c	M	M	GCAGCAGTGTTCTGGGTTAACAGGA	PWK: 593pb BALB: 796pb	
Foxk2-1r	121 324 653								GTCCTTTCAGCAGTCTGCCTCAGTT		
wdr45b-1f	121 344 547	c	c	c	M	c	M	M	GCAAGGTGGGCCAAACCAAGGTAAT	PWK: 315pb BALB: 506pb	
wdr45b-1r	121 345 052								GGCAGAAAAGGCCCGACTCACTTAA		
B3gntl1-1f	121 649 133	c	c	c	M	c	M	M	CCTCTCGGTCTGGTTGTTGGTGATC	PWK: 198pb BALB: 690pb	
B3gntl1-1r	121 649 822								CTCCCTCCACTAAGACAAGGCCCTA		
Metml-1f	121 711 717	c	c	c	M	c	M	M	TCATTGAAGAAGCCCAGGCCTTAGC	PWK: 228pb BALB: 674pb	
Metml-1r	121 712 390								ACTACCTCCTTCAGTTGTGCTTGGC		

* according to GRCm38-mm10

Table S2. Nucleotide and protein variants between the BALB/cJ and the PWK/PhJ strains in the *Rnf213* gene (Chr: 11:119,393,100-119,487,418).

Nucleotide variant*			Functional impact	Protein variant**	
Position	BALB	PWK		Position	Region
SNPs					
119,402,554	T	C	missense_variant	S44P	exon03
119,402,617	C	T	missense_variant	L65S	exon03
119,402,618	T	C	missense_variant	L65S	exon03
119,402,668	A	G	missense_variant	N82D	exon03
119,408,883	C	T	missense_variant	P146L	exon04
119,408,898	T	A	missense_variant	I151N	exon04
119,410,735	C	T	missense_variant	R345W	exon07
119,414,325	T	C	splice_region_variant	463	exon08/09
119,414,329	C	T	splice_region_variant	463	exon08/09
119,414,379	T	C	missense_variant	F479L	exon09
119414400	T	A	missense_variant	F86I	exon09
119,414,423	C	A	missense_variant	D493E	exon09
119,415,046	T	C	missense_variant	M560T	exon10
119,415,199	G	A	missense_variant	R611K	exon10
119,415,214	T	C	missense_variant	L616S	exon10
119,415,286	C	G	missense_variant	P640R	exon10
119,416,642	T	G	splice_region_variant synonymous_variant	709	exon11/12
119,418,153	A	G	missense_variant	M736V	exon12
119,420,089	A	T	missense_variant	Q811L	exon14
119,420,101	T	C	missense_variant	I815T	exon14
119,421,309	T	C	splice_region_variant	856	exon14/15
119,423,029	G	A	missense_variant	G918S	exon16
119,424,276	C	A	missense_variant splice_region_variant	Q982K	exon17/18
119,427,672	G	A	splice_region_variant	1098	exon19/20
119,428,055	G	A	missense_variant	R1113K	exon20
119,430,298	T	G	missense_variant	L1193I	exon21
119,430,520	T	C	missense_variant	V1267A	exon21
119,430,606	C	G	missense_variant	R1296G	exon21
119,431,730	C	G	missense_variant	A1391G	exon22
119,435,905	C	T	splice_region_variant	1575	exon25/26
119,436,016	A	G	missense_variant	R1610G	exon26
119,436,068	G	A	missense_variant	K1627S	exon26
119,436,069	T	G	missense_variant	K1627S	exon26
119,436,308	G	A	missense_variant	S1707N	exon26
119,436,397	A	G	missense_variant	S2052G	exon26
119,437,613	C	T	splice_region_variant	1957	exon26/27
119,437,800	A	G	missense_variant	I2920V	exon27
119,438,060	T	C	missense_variant	S2052P	exon28
119,440,315	G	A	missense_variant	V2117M	exon29
119,440,407	A	C	missense_variant	K2147N	exon29
119,440,554	G	T	missense_variant	K2196N	exon29
119,441,657	C	T	missense_variant	S2564F	exon29
119,441,675	A	G	missense_variant	N2570S	exon29
119,446,209	G	T	splice_region_variant	3352	exon31/32
119,449,331	A	G	missense_variant	T3462A	exon34
119,449,812	T	C	missense_variant	V3499A	exon35

119,460,010	T	G	missense_variant	H3889Q	exon42
119,467,227	A	C	missense_variant splice_region_variant	4268	exon49/50
119,479,673	A	G	splice_region_variant	4765	exon60/61
119,479,867	G	C	missense_variant	G4766A	exon61
119,480,890	C	A	missense_variant	N4839K	exon62
Indels					
119,409,459	C	CAGG	in frame	-262G	exon05
119,440,701	TGAA	T	in frame	E2246-	exon29
119,449,874	G	GGTAA	splice_region_variant	3519	exon35/36
119,467,356	C	CG	splice_region_variant	4307	exon50/51

* from the Sanger Institute Mouse Genomes Project (https://www.sanger.ac.uk/sanger/Mouse_SnpViewer/)

** according to the A0A171EBL2 sequence (https://www.uniprot.org/uniprot/A0A171EBL2)